多层氩弧熔敷含 TiC 颗粒增强涂层的微观组织及耐磨性能

宋思利， 邹增大， 王新洪， 李清明
（山东大学 材料科学与工程学院，山东济南 250063）

宋思利

摘 要：利用多层多道钨极氩弧熔覆技术，熔融预涂于钢基体表面钛铁和石墨混合粉末，可以在普通碳钢表面获得综合性能优异的复合材料表面熔敷层；测试和分析表明，熔敷层微观组织主要由铁素体、低碳马氏体、原位生成的 TiC 颗粒及碳化物等组成；熔敷层表面硬度达到了 HRC 57 以上，呈梯度分布特征；滑动磨损试验表明，由于 TiC 增强颗粒的存在，熔敷层与摩擦副的摩擦系数在磨损过程中不稳定，变化范围较大；TiC 颗粒对摩擦的阻碍、钉扎作用大大提高了熔敷层的抗磨损性能，熔敷层磨损体积比基体金属小 15～20 倍，具有良好的耐磨性能。

关键词：多层氩弧熔敷；熔敷层；微观组织；摩擦系数；耐磨性能
中图分类号：TG423 文献标识码：A 文章编号：0253－360X(2007)04－033－05

0 序 言

在矿山开采、重型冶金、油气钻探等工作领域，能够承受剧烈冲击及抗腐蚀、抗磨损成为机械零件的基本要求[1]，在耐磨部件表面熔敷具有特殊性能的金属基复合材料涂层成为这些领域修复部件、强化零件使用寿命的重要途径[2,3]。TiC 颗粒具有高硬度、高熔点和较好的热稳定性，在复合材料中多以微细颗粒析出，对基体金属的韧度损害较小，所以，用 TiC 颗粒增强的复合材料在耐磨领域应用前景广阔[4－6]，这使得制备含 TiC 颗粒增强的金属基复合涂层成为近年来表面工程领域的研究热点[7,8]。目前试验室多采用激光或等离子热源制备含 TiC 增强的复合涂层[9－11]，用钨极氩弧熔敷技术制备含 TiC 颗粒增强的复合材料耐磨涂层的研究和报道较少。由于钨极的载流能力有限，电弧功率受到限制，致使焊缝熔深比较浅，焊接速度低，这一工艺特点正适合用表面强化处理。

作者利用钨极氩弧热源，熔敷预涂在普通碳钢表面上的合金粉末，制备出含原位合成 TiC 增强的熔敷层，并对熔敷层的微观组织和磨损性能进行研究，探讨钨极氩弧熔敷技术制备含 TiC 颗粒增强涂层的工程应用。

收稿日期：2006－09－26
基金项目：教育部博士点基金资助项目(20020422032)

1 试验材料与方法

1.1 试验材料

熔敷试验的基体金属采用 Q235，试板尺寸为 200 mm×100 mm×10 mm，基体表面用角磨机和砂纸打磨，用无水酒精及丙酮清洗。熔敷粉末采用 FeTi25，纯度为 99.5%，200 目和石墨粉末（纯度为 99.9%，200 目），FeTi25 的主要化学成分见表 1。钛铁粉中 Ti 元素和石墨中的 C 元素按照摩尔分数比 Ti:C=1:1（质量分数比，Ti:C=47.88:12.01）配成混合粉末。混合粉末采用球磨混和，在球磨机中研磨 30 min 混合均匀，球磨时采用氩气保护。

表 1 FeTi25 的主要化学成分（质量分数，%）
Table 1 Chemical compositions of FeTi25

牌号	Ti	Al	Si	C	Fe
FeTi25	25.2	4.8	2.2	0.08	余量

1.2 试验方法

混合粉末采用丙酮稀释自制的粘结剂，将合金粉末粘结成糊状，预涂在经过处理后的试板上，在空气中自然干燥。

试验采用自动钨极氩弧焊机，焊枪安装在自动行走机构上；钨极采用直径为 2.5 mm 含 2%钍的钨极。为保证熔敷层的宽度和厚度以制备磨损试样，试验采用多层多道熔敷。各层各道均采用焊接电流

150 A, 熔敷速度 75 mm/min, 氩气流量 10 L/min; 每道熔敷前均空冷到室温; 各层各道间用手持角磨机打磨毛刺至金属光泽, 丙酮清洗, 自然风干。各层各道的熔敷试验参数见表 2。

表 2 熔敷试验参数

Table 2 Cladding parameters

层	道	电压 U/V	弧长 l/mm	预涂厚度 d/mm	平均厚度 $\bar{d}$/mm
第	1	13.5	4.4	1.7	
一	2	12.7	3.7	1.5	1.3
层	3	13.5	4.2	1.4	
第	1	12.5	3.6	1.5	
二	2	11.5	3.2	1.3	1.2
层	3	12.5	3.6	1.4	
第	1	13	4.1	1.2	
三	2	12.5	3.7	1.3	1.0
层	3	13	3.9	1.2	

1.3 试样制备与试验方法

沿焊缝横断面制作金相试样, 试样经研磨抛光后采用 5%的硝酸酒精腐蚀, 采用金相显微镜、扫描电镜对熔敷层进行组织观察, 采用 X 射线衍射仪进行物相鉴定, 利用洛氏硬度计测量熔敷层各部位硬度。

采用 MM —200 滑动磨损试验机进行磨损试验; 磨损试样尺寸为 10 mm× 10 mm×35 mm; 试样采用线切割, 磨损面经细磨抛光, 表面粗糙度 $R_a \leqslant 0.20\ \mu m$。

2 试验结果与分析

2.1 熔敷层的相组成

图 1 给出了熔敷层表面层的 X 射线衍射谱线。衍射谱线出现了 α－Fe, TiC, Fe_3C 的衍射峰, 这表明熔敷层已生成一定数量的 TiC 颗粒, 同时也生成了一些渗碳体颗粒。

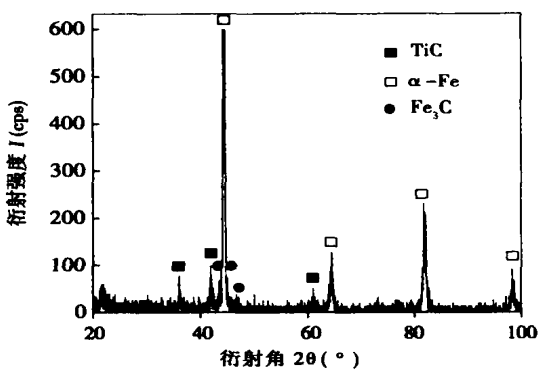

图 1 熔敷层表面的 X 射线衍射图样

Fig. 1 XRD spectra of superficial layer in coating

2.2 熔敷层微观组织分析

利用金相显微镜对熔敷层进行微观组织观察。熔敷层内未见裂纹、气孔、夹杂等缺陷。熔敷层与基体金属表面形成的熔合区晶粒以半熔化母材的基本晶粒为核向熔敷层内生长, 形成垂直于熔合线指向熔敷层的柱状铁素体晶粒。熔敷层与碳钢基体为良好的冶金结合, 如图 2 所示。

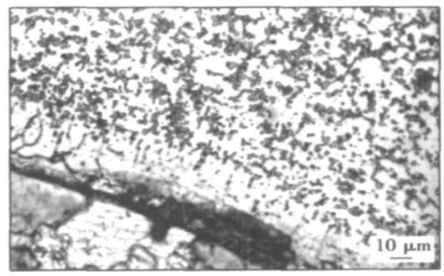

图 2 基体及熔合区微观组织

Fig. 2 Microstructure of fusing zone

图 3, 图 4 给出了熔敷层一、二层和靠近表层区域的微观组织形貌。由图可以看出, 熔敷层的微观组织主要由铁素体、低碳马氏体和 TiC、碳化物颗粒等组成, 见图 3。熔敷层呈现距离熔敷层表面越近, 低碳马氏体、TiC 颗粒和碳化物的体积分数越多的组织特征, 这主要是熔敷层的 C 元素被基体金属稀释程度变小所致。随着距离表层越近, C 元素的含量越高, 越容易形成低碳马氏体组织和碳化物, 使得熔敷层硬度增大, 韧度变差, 见图 4。

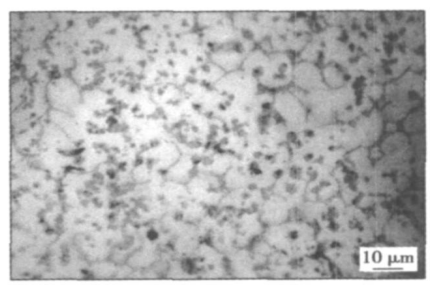

图 3 熔敷层中间区域的微观组织

Fig. 3 Microstructure of Intermediate zone in coating

试验研究采用的是多层多道熔敷的方式获得熔敷层, 这种工艺条件下, 由于后熔敷的焊道对前面的熔敷层有一个热处理和部分重熔的过程, 熔敷层内的 TiC 初生枝晶在热处理和重熔过程中也发生了熔断和粒化现象, 形成了颗粒状或短棒状的 TiC 颗粒,

在复杂的热处理过程中也发生了聚集长大现象，使 TiC 的颗粒形态和数量也呈现出梯度分布的特征，即在熔敷层的中间区域，TiC 颗粒呈弥散分布，颗粒尺寸较小。而靠近熔敷层表面则出现了数量较多、尺寸较大的TiC 颗粒，如图 4 所示。

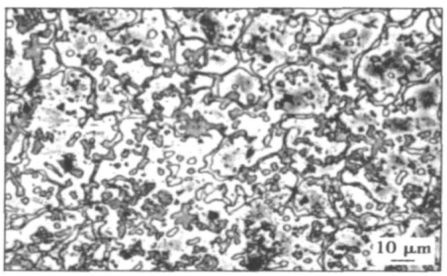

图 4　熔敷层表面区域的微观组织

Fig 4　Microstructure of superficial zone in coating

3　熔敷层的表面硬度及磨损性能

3.1　熔敷层的表面硬度

一般来说，材料的硬度和耐磨性能有密切的关系，其表面硬度高的材料耐磨性能也很优异。因此，提高熔敷层的表面硬度对提高材料的耐磨性能有很重要的工程意义。表 3 给出了熔敷层表层各点的硬度(HRC)测量结果。由表可知，试验中获得的熔敷层表面硬度达到了 57HRC 左右，比基体的表面硬度高出一倍以上。

表 3　熔敷层表面宏观硬度(HRC)

Table 3　Hardness of coatings (HRC)

数值 1	数值 2	数值 3	数值 4	数值 5	数值 6
61.5	61	57	60	57.5	52.5
数值 7	数值 8	数值 9	数值 10	数值 11	平均值
56.5	58	54.5	57	59	57.6

3.2　熔敷层的磨损试验

熔敷层的磨损试验采用滑动磨损试验机 MM 一200。磨轮外直径 40 mm，磨轮材料为经过调质处理的W18Cr4V 工具钢，硬度为 62HRC；磨轮转速 200 r/min；磨损试样为长方体，尺寸为 10 mm×10 mm×35 mm；摩擦面经磨削加工后研磨抛光，表面粗糙度 $Ra \leqslant 0.20\ \mu m$。磨损试验时分别采用载荷为 5，10 kg 对基体和熔敷层分别磨损两次；母材磨损时间为 5 min，熔敷层磨损时间 20 min；试验过程中每间隔 10 s 测定摩擦系数，每间隔 5 min 测定一次磨痕宽度。采用式(1)计算得出磨损体积

$$V = L\left(R\arcsin\frac{b}{2R} - \frac{b}{2}\sqrt{R^2 - \frac{b^2}{4}}\right), \qquad (1)$$

式中：V 为磨损体积；L 为试样宽度；R 为磨轮半径；b 为磨痕宽度。

图 5 给出了载荷为 10 kg，磨损时间分别为 5，20 min的熔敷层和母材的磨损摩擦系数随时间变化的曲线(熔敷层表层只截取前 5 min 的曲线图)。由图对比可以看出，母材的摩擦系数变化幅度较小，基本数值在 0.5～0.7 之间变化，波动范围小，表现出较为稳定的摩擦过程。

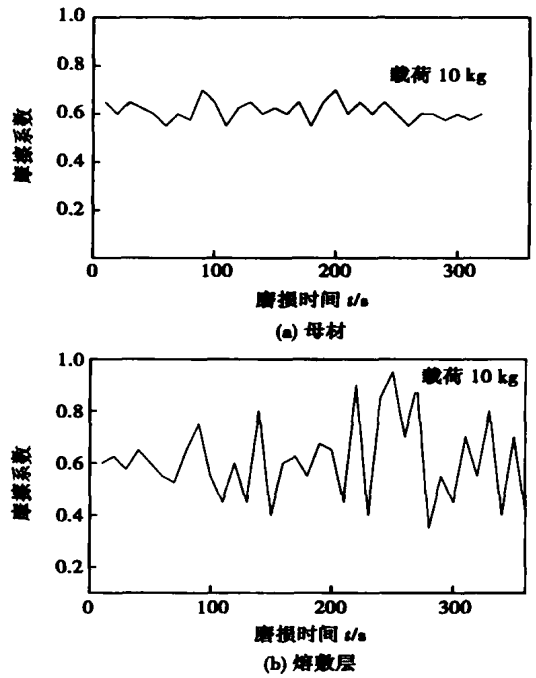

图 5　母材和熔敷层表层摩擦系数—时间曲线

Fig 5　Curve between frictional coefficient and time of base metal and coatings

而对于熔敷层来说，由于TiC 耐磨质点的存在，当暴露于摩擦面表面的 TiC 颗粒与摩擦副之间产生相对运动时，必须克服由于 TiC 颗粒而增加的阻碍，使得摩擦力增加，摩擦系数增大。由于熔敷层表面的 TiC 颗粒尺寸较大，分布不均与，这些摩擦平台使得摩擦过程极不稳定，摩擦系数波动范围加大。这种 TiC 颗粒对摩擦的阻碍、钉扎作用大大提高了熔敷层的抗磨损性能。

3.3　熔敷层表层的磨损体积对比

与基体金属相比，熔敷层表现出良好的耐磨性能，图 6 给出了熔敷层表层磨损体积随磨损时间增加的曲线；图 7 给出了同样磨损条件下基体金属与

熔敷层磨损体积的对比柱形图，由图可以看出，熔敷表层的磨损体积随磨损时间的增加而增加；同样磨损条件下，熔敷表层的磨损体积只有基体母材的 1/15～1/20，也就是说，熔敷表层的耐磨性能是基体的 15～20 倍。

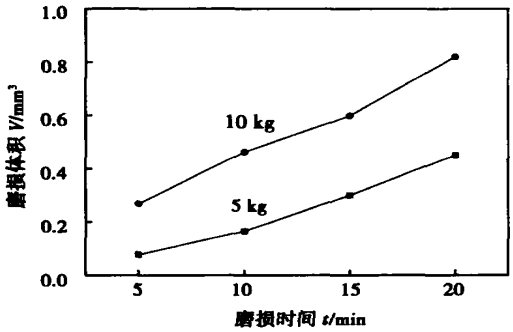

图 6 熔敷层磨损体积—时间曲线

Fig. 6 Wearing volume-time curve of coatings

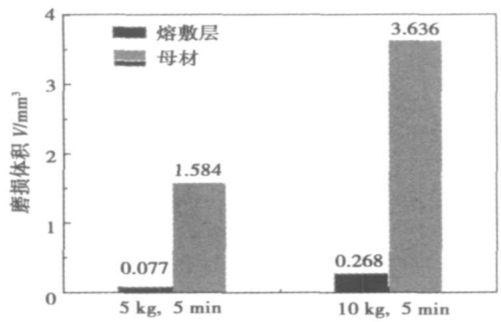

图 7 熔敷层与基体磨损体积对比

Fig. 7 Comparison of wearing volume between base metal and coating (wearing time= 5 min)

3.4 磨痕的扫描电镜(SEM)观察分析

图 8，图 9 给出了熔敷层、母材分别在法向载荷为 10 kg，磨损时间分别为 5，20 min 磨损条件下的磨痕电子扫描 SEM 图片。由两图可以看出，熔敷层表层由于耐磨硬质点的存在，阻碍了磨痕的发展，磨痕在硬质点前被阻断，TiC 颗粒暴露于摩擦表面，与经显微犁削而变形移位在 TiC 颗粒前堆积的基体金属形成一个阻磨平台或小丘。磨痕始于耐磨质点的后面而止于下一个耐磨质点前，犁沟短而浅，见图 8；而对于母材金属，由于没有了硬质点的存在，犁沟宽且深而长，一直贯彻于整个摩擦面，没有阻断和断续现象，见图 9。由此得知，由于耐磨硬质点如 TiC 颗粒等的存在，使熔敷层的磨损性能大大优于母材金属。

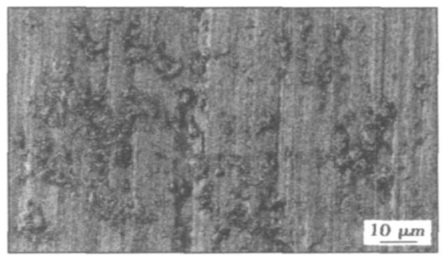

图 8 熔敷层的磨痕形貌(SEM)

(载荷 10 kg，磨损时间 20 min)

Fig. 8 SEM photo of wear trace on coating

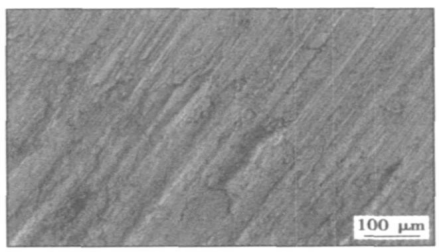

图 9 母材的磨痕形貌(SEM)

(载荷 10 kg，磨损时间 5 min)

Fig. 9 SEM photo of wear trace on base metal

4 结 论

(1) 利用钨极氩弧熔敷钛铁和石墨粉末，可以在熔敷层中反应原位合成 TiC 颗粒；随着熔敷层位置的不同，TiC 呈梯度分布特征，以颗粒状、块状或花瓣状弥散存在于熔敷层组织中。

(2) 熔敷层的表面硬度较高，试验平均硬度达到 HRC 57 以上；由于耐磨硬质点 TiC 颗粒的存在，熔敷层的摩擦系数波动幅度加大，具有良好耐磨性能，比基体金属提高 15～20 倍以上。

(3) 采用多层钨极氩弧熔敷工艺，在 Q235 钢基体表面原位合成了 TiC 颗粒增强的耐磨熔敷层；熔敷层与母材是良好的冶金结合，无裂纹、夹杂、气孔等缺陷。

参考文献：

[1] 徐滨士，朱绍华. 表面工程的理论与技术[M]. 北京：国防工业出版社，1999.

[2] 王新洪，邹增大，宋思利，等. TiC—VC 免预热耐磨堆焊焊条[J]. 焊接学报，2002，23(4)：31—34.

[3] Xu binshi，Zhang wei，Xu weipu. Influence of oxides on high velocity

arc sprayed Fe－Al/Cr－3C－2 composite coatings[J]. Joural of Central University of Technology, 2005, 12(3): 259－262.

[4] 宋思利，王新洪，邹增大. TiC 增强铁基堆焊层组织与性能的研究[J]. 山东大学学报(工学版)，2004，34(2)：1－5.

[5] 陈寒元，邹正光，麦立强，TiC 复合材料的研究进展[J]. 粉末冶金工业，2001，11(3)：38－44.

[6] Wang xinhong, Song sili, Zou zengda, *et al*. Development of new type of wear and crack resistant hardfacing electrode[J]. Transactions of Nonferrous Metals of China, 2004, 14(4): 660－664.

[7] 严有为，魏伯康，林汉同. 原位 TiC 颗粒增强灰铸铁复合材料的组织及摩擦磨损性能[J]. 摩擦学学报，2003，23(4)：37－41.

[8] Wang xinhong, Zou zengda. Effect of rare earths on microstructure and properties of TiC－based cermet/Cu alloy composite wear resistant materials[J]. Joural of Rare Earths, 2003, 21(3): 375－379.

[9] 吴玉萍，彭竹琴，林萍华. 等离子原位合成 TiC 颗粒增强 Ni 基复合涂层[J]. 材料科学与工艺，2004，12(4)：429－432.

[10] 王新洪，张　敏，邹增大，等. 激光熔覆 TiCp/Ni 基合金复合涂层的显微组织与性能[J]. 机械工程学报，2003，39(2)：37－42.

[11] 田永生，陈传忠，王德云，等. 激光熔覆生成碳硅钛化合物及其组织性能研究[J]. 中国激光，2004，31(7)：879－882.

[12] 赵宇光，蒋启川，任露泉，等. Fe－C－Ti－Mn 合金系 TiC 原位生成反应的热力学分析[J]. 吉林大学学报(工学报)，2004，123(1)：201－205.

作者简介：宋思利，男，1970 年出生，博士研究生，助理研究员。主要从事焊接冶金及金属表面工程方面的科研工作。在国内外期刊发表论文 10 余篇。

Email：ssl1970@sdu.edu.cn

[上接第 32 页]

[2] Froes F H. The Science technology and applications of magnesium[J]. JOM, 1998, (9): 30－33.

[3] 樊　丁，黄　勇，张瑞华，等. 均匀设计法在铝合金 A－TIG 活性剂配方研制中的应用[J]. 甘肃工业大学学报，2003，29(2)：5－7.

[4] Liming liu, Zhaodong zhang, Gang song, *et al*. Effect of cadmium chloride flux in active flux TIG welding of magnesium alloy[J]. Materials Transactions, 2006, 47(2): 446－449.

[5] 陈　俐，胡伦骥. 活性剂焊接技术的研究[J]. 新技术新工艺，2005，4：39－42.

[6] 刘全坤. 材料成形基本原理[M]. 北京：机械工业出版社，2004.

[7] Howse D S, Lucas W. Investigation into arc constriction by active fluxes for tungsten inert gas welding[J]. Science and Technology of Welding and Joining, 2000, 5(3): 189－193.

[8] 任雪婷. 不锈钢单组分活性剂 A－TIG 焊规范及活性机理的研究[D]. 大连：大连交通大学，2004.

作者简介：刘黎明，男，1967 年出生，教授，博士生导师。主要研究方向：焊接新材料及焊接自动化。获省部级发明奖 3 项，发表论文 70 余篇。

Email：liulm@dlut.edu.cn

finite element numerical simulation

Process of $(Cr, Fe)_7C_3$/γ — Fe ceramal composite coating formed by plasma surface metallurgy LIU Junbo (School of Mechanical and Electronic Engineering, Weifang University, Weifang 261061, Shandong, China). p17—20

Abstract: The effect of process parameters on the $(Cr, Fe)_7C_3$/γ—Fe ceramal composite coating formed by plasma surface metallurgy on Q235 steel substrate was researched. With the increase of scanning speed or decrease of working current, microstructure of coating was refined. Therefore, it can be ascertained that the optimum working current is 300 A and the optimum scanning speed is 500 mm/min. A in situ reinforcing phase $(Cr, Fe)_7C_3$ ceramal composite coating was fabricated on substrate of Q235 steel by plasma surface metallurgy with the Fe—Cr—C—Nb—Al alloy powders. The ceramal composite coating has a rapidly solidified microstructure consisted of primary $(Cr, Fe)_7C_3$ and the $(Cr, Fe)_7C_3$/γ—Fe eutectics, and is metallurgically bonded to Q235 steel substrate.

Key words: plasma surface metallurgy; process parameters; microstructure; microhardness

Medelling and simulation of resistance spot welding inverter JI Chuntao, PENG Xin, LUO Xianxing, DENG Lipeng (Material Science and Engineering School, Nanchang Institute of Aeronautical Technology, Nanchang 330034, China). p21—24

Abstract: The simulation tool in Matalab was used to characterize the resistance welding inverter system and to optimize the circuit parameters. The system output waveforms were analyzed and simulated for different filter capacitors and secondary loads. The result shows that the filter capacitor should be selected so that the rectifier output current is intermittent pulsative, and load current is supplied by the rectifier at voltage crest and by the capacitor at voltage trough. The secondary current rises as exponential fuction and its rising rate is a inverse proportional to the secondary inductance. It will finally reach a maximum value which is not affected by the inductance when provided the welding time is long enough.

Key words: resistance welding; inverter; system simulation

Microstructure and properties of welded joint for narrow gap laser welding of 42CrMo steel bevel gear shaft WU Shikai, YANG Wuxiong, DONG Peng, XIAO Rongshi (National Center of Laser Technology, Beijing University of Technology, Beijing 100022, China). p25—28

Abstract: The manufacturing of a heavy type bevel gear shaft is generally machined separately, and then jointed by welding. Aimed to the joining of the quenched and tempered 42CrMo steel bevel gear shafts for a heavy-duty machine, a 3500 W Slab CO_2 laser was applied and narrow gap laser welding process was adopted with filler wire of TGS—2CM. Meanwhile, the performance and metallographic structure of the joint were studied. The experiment results demonstrate that there are no cracks and porosities in the joint even without preheating and postweld heat treatment when the appropriate laser welding parameters are used. The microstructure in the weld and heat-affected zone is fine bainite. The micro-hardness of fusion area is about 580HV0.2, and no apparent softened zone exists in the welded joint. The tensile strength of the joint is in 980—1080 MPa, and equivalent to that of the base material, which is satisfied with the service demand.

Key words: laser welding; narrow gap; 42CrMo steel; bevel gear shaft; joint properties

A—TIG welding of magnesium alloy with activating welding wire LIU Liming, CAI Donghong, ZHANG Zhaodong, ZHU Meili (State Key Laboratory of Materials Modification & School of Materials Science and Engineering, Dalian University of Technology, Dalian 116024, China). p29—32, 37

Abstract: Several single common compounds were taken as basic activating fluxes in the tungsten inert gas (TIG) welding process with filler wire. The results indicated that in A—TIG welding of magnesium alley, the activating fluxes coated on the welding wire can also increase weld penetration. The chloride shows a prominent effect on the weld penetration, and the penetration even can be increased 3 times, which compared with the conventional TIG welding with filler wire. The boiling points of the fluxes that increased weld penetration are mostly in the regions about 900 ℃. The interfusion ability between the droplet metal and the weld pool metal became worse in the TIG welding process with filling activating welding wire than that with the normal wire, and filling ability of the welding wire deteriorates a little, comparing with the normal welding mire.

Key words: activating welding wire; activating fluxes; welding wire filling ability

Microstructure and wear-resisting property of TiC particle reinforced coatings cladded by TIG welding with multiple layer SONG Sili, ZOU Zengda, WANG Xinhong, LI Qingming (School of Materials Science and Engineering, Shandong University, Jinan 250061, China). p33—37

Abstract: By using TIG welding, ferrite based composite coating reinforced with TiC has been synthesized by preplaced alloy powder which contains Ti and C on the surface of conventional carbon steel. Results show that in situ TiC particles were prepared in the coating. The microstructure of the coating was mainly composed of ferrite, retained austenite, TiC particles and carbide. The surface hardness of the coating is higher than 55 HRC and presents gradient distribution nearer to the surface of the coating. The wear-resisting test indicated that the friction coefficient of the coating is varied acutely. Blocking effect of TiC particles leads to excellent wearing resistance. The coating has a excellent wear-resisting property. The

result of wear-resisting test shows that the wear-resisting volume of the coating is less than that of the base metal by 15—20 times.

Key words: tungsten inert-gas welding; coating; TiC particle; microstructre; wear-resisting property

Edge detection of metal transfer image based on wavelet transform YANG Qian, WANG Guangwei, HUA Xueming, WU Yixiong (Material Science and Technology Department, Shanghai Jiaotong University, Shanghai 200030, China). p38—40

Abstract: Wavelet transform and improved Prewitt operator were used to detect the edge of the droplet image in GMAW. After preprocessing, wavelet transform was used to perform decomposition to different detailed levels, and enhance diagonal detail coefficients by multiplying it with the proper parameters, then reconstruct image. Improved Prewitt operation was used to detect the edge of reconstructed image. The experiment results demonstrate that the method is effective to detect the real outline of droplet and real edge of weld pool, and the levels of decomposition and the multiples are vital factors, which depends on the real image.

Key words: wavelet transform; improved Prewitt operator; metal transfer; image processing; edge detection

Electron beam welding of dissimillar metal between Ti—43Al—9V—0.3Y and TC4 ZHANG Binggang, CHEN Guoqing, HE Jingshan, FENG Jicai (National Key Laboratory of Advanced Welding Production Technology, Harbin Institute of Technology, Harbin 150001, China). p41—44

Abstract: The morphology of welded joint between Ti—43Al—9V—0.3Y and TC4, the phase composition and the effect of the welding parameters on the tensile-strength are analysed. The weld zone is mainly composed of the coarse columnar crystals, and its phase composition includes Ti_3Al, TiAl, B2 and YAl_2. The columnar crystals in the weld near TC4 are grown up from the grains of the base metal, and the equiaxed grains in the heat-affected zone are coarse $\alpha+\beta$ structure, and the sizes of the two kinds of grains are distinct. The weld near TiAl is a corrosion resisting bleached zone, and it is composed of single B2 phase. The effect of the welding parameters on the tensile strength of the joint was analyzed. The results shows the welding speed has little influence on the tensile strength, a peak of the tensile strength appears with the change of seam current. the maximum of the tensile strength of the weld is 209.8 MPa in the tested range.

Key words: TiAl-based alloy; TC4 alloy; electron beam welding

Effect of welding parameters on microstructure and mechanical propertes of welded joint in PAW of SiCp/6061Al LEI Yucheng, ZHU Fei, YUAN Weijin, CHENG Xiaonong (School of Material Science and Engineering, Jiangsu University, Zhenjing 212013, Jiangsu, China). p45—48

Abstract: The weldability of SiCp/6061Al MMCs was studied with plasma arc welding. The effect of welding parameters (welding current, welding speed) on the microstructure and mechanical properties of welded joint with and without filler Ti was investigated. The results showed: Without the filler Ti, the welding parameters can only change the dimension and quantities of Al_4C_3 which is the harmful particles, but not restrain its generation; with the filler Ti, types and distribution of reinforcement phase are the main factors to affect the mechaical properties of welded joint. Adjusting the welding parameters properly is beneficial to form a completely new in-situ section with the TiC TiN and AlN as the reinforced particles can be formed at the weld center. Meanwhile the width of the old and new reinforced phases coexistence is reduced and the segregation of reinforced SiC particles is eliminated, thereby the mechanical properties of welded joints is enhanced.

Key words: plasma arc welding; metal matrix composites; welding parameters; microstructure; mechanical properties

Low power laser welding of magnesium alloy with activating flux SUN Hao, ZHANG Zhaodong, LIU Liming (State Key Laboratory of Materials Modification & School of Materials Science and Engineering, Dalian University of Technology, Dalian 116024, China). p49—52, 57

Abstract: The behavior of the laser welding of magnesium alloy with several activating fluxes was studied under the same experimental condition. The results show that the addition of oxide and chloride activating fluxes can increase weld penetration and D/W (depth/width) ratio in the condition of low power laser welding. The flux SiO_2 can make the penetration increased as much as 220%. It is proved that the activating flux can be used to increase weld penetration and decrease the cost of laser welding of magnesium alloy thin plate. It is found that the heat input has a large influence on the increment of the weld penetration. The main reason for the increment of laser absorptivity is that fluxes absorb more laser energy and transmit it to the specimen during the early period of laser action.

Key words: magnesium alloy; laser beam welding; activating flux; oxide

Processing technology of process data based on WCAPP QIAN Xiaojun[1], SHEN Chunlong[1], WANG Kehong[2] (1. Department of Computer, Nanjing Normal University, Nanjing 210097, China; 2. Department of materials, Nanjing University of Science & Technology, Nanjing 210094, China). p53—57

Abstract: On the base of analyzing process data representing and operation properties, the structure of welding structure product hierarchy information Mode/View/Control was built. The expression and operation of model was described. Parameter data of welded joint, master parameters and information of welded joint were inte-